Growth of Highly Oriented Deuterium Crystals in Silicon Nanochannels

T. Hofmann,[1,*] P. Kumar,[2] M. Enderle,[3] and D. Wallacher[1]

[1]*Helmholtz-Zentrum Berlin für Materialien und Energie GmbH, Hahn-Meitner-Platz 1, D-14109 Berlin, Germany*
[2]*Department of Physics, National Institute of Technology Delhi, Delhi 110077, India*
[3]*Institut Laue-Langevin, BP 156, 38042 Grenoble Cedex 9, France*

(Received 4 September 2012; revised manuscript received 10 December 2012; published 7 February 2013)

The structure of solid deuterium confined in 9 nm wide tubular silicon nanochannels has been studied by means of elastic neutron scattering techniques. As a result we report the formation of fcc D_2 as the stable solid phase in confinement in contrast to the hcp bulk structure. Further, a preferred alignment of D_2 nanocrystals with respect to the surrounding crystalline silicon matrix is discussed in terms of hetero-epitaxial growth of solid D_2 on crystalline pore walls.

DOI: 10.1103/PhysRevLett.110.065505 PACS numbers: 61.46.Hk, 61.05.fm, 61.43.Gt

In recent years, nanostructured templates emerged as a versatile tool to define the morphology of functional materials on nanometer-sized length scales [1–9]. Numerous publications reported improved functionality in materials tailored by means of nanopatternd substrates. Imprinting of nanopatterns in poly(3-hexylthiophene) (P3HT) layers manipulated their microscopic structure and hence was expected to improve the performance of organic solar cells [2]. Metallic nanowires in anodized Si were grown to exhibit fascinating magnetic properties [3]. Metal-semiconductor nanocompounds were discussed for utilization in spintronic and magnetic applications [4]. Enhanced charge collection was found in pore-confined organic solar cells [5] and mesoporous alumina membranes were employed to grow well-aligned bundles of liquid crystalline nanowires [9].

In many of these experiments the crystallization inside a nanometer-sized confining template is the structure and thus performance defining process. In detail, confinement effects, fast growing crystal directions [10], and interfacial energies at the host-guest interface [2] are considered to guide crystal nucleation and growth. Less is known on the impact of the host's microscopic structure, e.g., roughness and crystallographic facets on the solidification process [11].

Structure, texture, and polymorphism control in nanostructured devices is of huge technical impact and should benefit greatly from a thorough understanding of solidification processes in confinement. As metal deposits in nanoconfinement or structured polymers are more challenging endeavors [2,3] in terms of fabrication, pore condensed and solidified gases provide a more feasible route for studies that elucidate the basic principles of solidification in confinement. Rare gases, hydrogen isotopes, nitrogen, etc., exhibit the most fundamental structures hcp and fcc representative for many metallic systems; they interact via dispersion forces and are easily condensed in porous matrices and structurally probed by means of elastic neutron scattering techniques.

Here we present a crystallization study on one of the hydrogen isotops, deuterium D_2 in a crystalline porous silicon matrix. Depending on temperature and spin isomer composition, its molecular crystals exhibit arguably the most fundamental center of mass stacking sequences in nature hcp and fcc. We report a comprehensive neutron scattering study on confined deuterium (cD_2) in an regular array of nanochannels in porous silicon (pSi). In contrast to structural studies, which utilize substrates with randomly oriented pore networks, the array of well-aligned nanochannels provided the unique opportunity to ascertain the crystallographic structure of cD_2 as well as to discern preferred growth directions of nanocrystals inside the confining host. Like other quantum systems, hydrogen isotopes have been studied before in confinement [12–21]. However, structural studies have been abandoned early [21].

Anodization of bulk silicon in hydrofluoric acid [22] allowed us to etch 250 μm thick mesoporous layers in 500 μm thick single crystalline (001) silicon wafers. The chosen set of anodization parameters [22] facilitated the growth of noninterconnected tubular nanochannels along the [001]-direction of the silicon crystals with a average diameter of 9 nm at a total porosity of $\sim$50%. In total twenty mesoporous silicon plates (10 mm $\times$ 20 mm) were prepared to provide sufficient pore volume ($\sim$ 0.5 cm^3) for the scattering experiments.

The pores were filled *in situ* at the neutron diffractometer with liquid D_2 at $T = 21.5$ K by means of a volumetric controlled sorption technique [23]. A well-defined sequence of adsorption and desorption steps related the fractional filling $f = N/N_0$ of the pores to the reduced pressure P/P_0 in the sample cell. Hereby, P and P_0 represent the vapor pressure of the pore condensate and the corresponding bulk system. N and N_0 are the uptake of D_2 in the pores and the number of molecules required to fill the pore space.

For scattering experiments the accumulated pore volume was filled at 21.5 K up to $f = 0.85$ with liquid D_2. The

remaining, empty pore space served as buffer for coexisting D_2 vapor in the excess volume of the sample cell [23], which condenses or sublimes as the sample is cooled down to 1.7 K to solidify the cD_2. Elastic scattering of thermal neutrons ($\lambda_{E6} = 2.44$ Å, $\lambda_{IN20} = 2.09$ Å) was utilized at diffractometer E6 of the Helmholtz Center in Berlin and spectrometer IN20 of the Institute Laue Langevin in Grenoble to elucidate the structure of the solidified cD_2. Scattering intensity was recorded in a plane that coincided with a $(\bar{1}10)$ plane of the crystalline silicon substrate (inset Fig. 2). For this purpose the symmetry axis of the tubular pores—the [001] direction of the substrate—and a [110] direction resided in the scattering plane. Intensity $I(2\theta, \omega)$ was recorded as function of scattering angle 2θ and substrate orientation ω, that is the angle in the scattering plane as defined by the [110] direction and the direction of the incoming neutrons.

The measured adsorption-desorption cycle in porous silicon (Fig. 1) resembles the typical shape of sorption isotherms known from van der Waals liquids [24]. At low pressures, that is $P/P_0 < P_{ad} = 0.75$ in adsorption respectively $P/P_0 < P_{de} = 0.6$ in desorption, D_2 physiosorbs on the pore walls [25]. At higher pressures in the hysteretic regime capillary condensation in the pore center is observed [25,26]. Pore condensed D_2 is thermodynamically stable at low temperatures well below the bulk saturation pressure.

Figure 2 exhibits the elastic scattering signal from cD_2 in pSi at $T = 1.7$ K. Intensities $I(2\theta, \omega)$ are combined to create a linear intensity map $I(Q_{001}, Q_{110})$ in reciprocal space. Here, Q_{001} and Q_{110} depict wave vector transfers along the Si surface normal and along the [110] in-plane direction, $\Phi^* = \omega - \theta$ defines a subsequently useful polar angle. The intensity distribution in the map manifests primarily anisotropic Bragg scattering from solid D_2 inside the pores as scattering contributions from the polycrystalline aluminum sample cell and the single crystalline silicon substrate have been subtracted as background. Scattering angles $2\theta_{fcc}$ can be readily assigned to (111), (002), (220), (113), and (222) reflections of a face centered cubic (fcc) structure with a lattice constant of $a_c = 5.16$ Å that is sizably strained compared to the bulk value of $a_b = 5.08$ Å [27]. The existence of the $(002)_{fcc}$ reflection, which is not shared between fcc and hcp structures and the absence of hcp $(100)_{hcp}$ and $(101)_{hcp}$ reflections forbids the assignment of a hcp structure and unambiguously evidences the fcc structure. Along rings of constant scattering angles $2\theta_{fcc}$ in Fig. 2, each fcc reflection is present with varying intensity at several but discrete angles Φ^*. Hereby, most intense scattering for a given scattering angle $2\theta_{fcc}$ is persistently found in direct vicinity of Si Bragg reflections as marked by symbols. Marked positions present $(111)_{Si}$, $(311)_{Si}$, $(220)_{Si}$, $(004)_{Si}$, respectively, symmetry equivalent Si reflections in a cubic unit cell ($a_{Si} = 5.43$ Å).

A subset of the recorded scattering data is shown in Fig. 3. The plot exhibits cuts in the intensity map along lines of constant wave vector transfer Q_{fcc}. The dependence of the scattering intensity on Φ^* is shown for (111), (002), (220), and (113) reflections. The existence of discrete reflections rather than Φ^* independent intensities as expected for Debye-Scherrer rings indicates a strong correlation between the crystallographic orientation of solidified cD_2 and the spatial orientation of the pores.

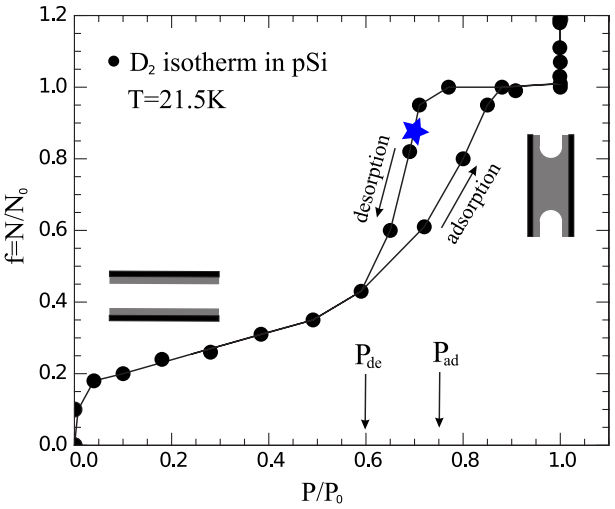

FIG. 1 (color online). Sorption isotherm for D_2 in pSi at $T = 21.5$ K: The fractional filling of the pores $f = N/N_0$ relates directly to the reduced pressure P/P_0. Arrows mark adsorption and desorption branch. Insets show different geometric distribution of the condensate depending on P/P_0. A star depicts the state of filling employed in scattering experiments.

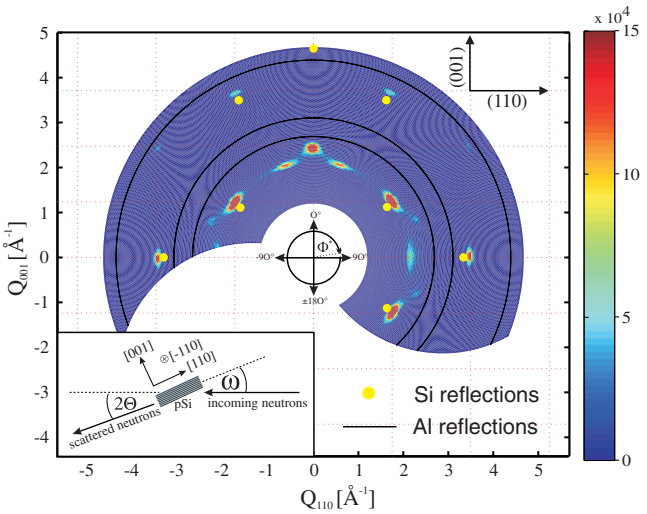

FIG. 2 (color online). Scattered intensity in the $(\bar{1}10)$-plane, recorded with a Si-mono-flatcone detector at IN20. Background scattering from Si wafers and Al sample cell are subtracted. Q_{110} and Q_{001} depict wave vector transfers in the [110] direction of Si crystals respectively along the [001] surface normal. The inset illustrates the scattering geometry.

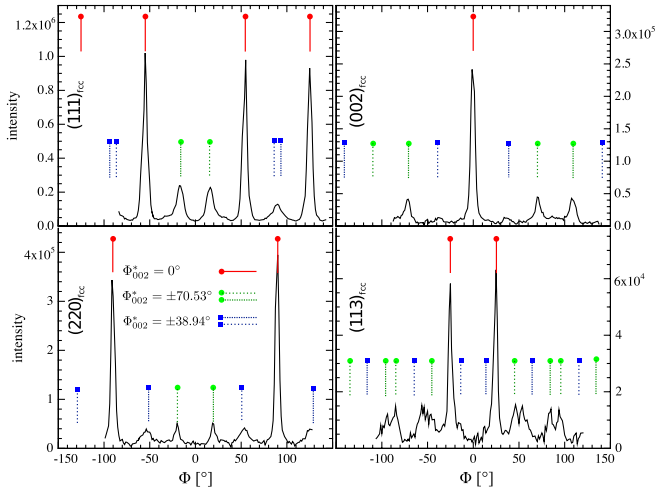

FIG. 3 (color online). Intensities are shown for (111), (002), (220), and (113) fcc reflections as function of Φ^*. Symbols denote Bragg reflection positions as expected for epitaxialy grown D_2 ($\Phi^*_{002} = 0°$), respectively, first and second order twins ($\Phi^*_{002} = \pm 70.53°$, $\Phi^*_{002} = \pm 38.94°$).

An analysis of the rocking curves in Fig. 3 leads to the conclusion that solid D_2 crystals in the nanochanels can be divided into a finite number of subsets. Each subset is characterized by a well-defined orientation of the D_2 crystals with respect to the surrounding single crystalline silicon matrix. Based on the reflection intensities in the different subsets, roughly 70% of the observed crystals align inside the pores perfectly with the crystallographic orientation of the single crystalline substrate. This subset is subsequently referred to as the aligned domain. The remaining 30% of the observed crystalline material, that are rotated domains, forms crystals in which the $(\bar{1}10)$ D_2 plane still coincides with the $(\bar{1}10)$ Si plane but is rotated by well-defined angles of approximately $\pm 71°$ and $\pm 39°$.

The temperature dependence of the intensity of various Bragg reflections as depicted in Fig. 4 shows that the cD_2 solidifies around 14 K and melts at 15 K. Both temperatures are well below the bulk triple point ($T^3 = 18.73$ K). The T dependence of the intensity resembles convincingly the behavior found for other pore condensates [28] as the sample is cycled through the liquid-solid phase transition (Fig. 4). Reduced transition temperatures with respect to the bulk system as well as a pronounced freezing-melting hysteresis could be reproducibly ascertained.

At all temperatures below the liquid-solid transition point the structure of the confined solid was identified as fcc. In contrast, bulk D_2 forms always a hcp phase right after freezing and only if the para content is sufficiently high ($> 56\%$) quadrupolar interactions trigger a cubic Pa3 phase below 3.8 K [29]. Such a high para content in the pore condensed hydrogen can be excluded, since normal D_2 with an equilibrium isomer composition of maximum 33% para hydrogen has been used in the experiment. We rather prefer to explain the difference in the phase sequence between the confined and bulk system from the marginal energy difference between fcc and hcp structures [30]. A preferred formation of fcc nanocrystals over hcp ones solely due to lower surface energies has already been proposed by Borden [31]. Both constraints, growing nanometer-sized solid nuclei as well as the structural mismatch between substrate and solid pore condensate, contribute to the free energy of the system in the porous host in favor of the cubic structure. The last issue is addressed in succeeding paragraphs, which promote that a fcc unit cell adapts better to the cubic silicon host than a hexagonal unit cell as it grows in an epitaxial fashion on the pore walls.

Concerns that D_2 in pSi might migrate out of the pore space while cooling to form an epitaxial grown solid on the external surfaces of the Si substrate were dispelled by the reduced liquid to solid transition temperatures as depicted in Fig. 4 and by scattering experiments performed on D_2, which solidifies in the presence of nonporous crystalline silicon wafers. Here, always the formation of a hexagonally close-packed powder at the bulk solidification temperature was observed.

A more comprehensive understanding of the directed domain growth requires a thorough treatment of crystal nucleation and growth phenomena in the nanochannels. Our experiments imply liquid phase epitaxy [32] inside the nanochannels as the primary structure and texture defining process and promote the following solidification sequence. First fcc seed crystals nucleate at the interface between supercooled liquid and solid pore walls to adapt the cubic structure of the single crystaline silicon matrix. Then the nuclei grow in size and guide an epitaxial solidification as the liquid-solid interface proceeds towards the pore center.

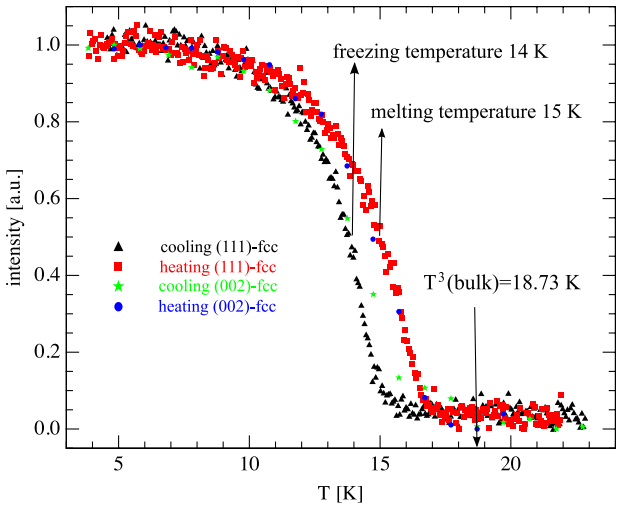

FIG. 4 (color online). Scattering intensity in various reflections as a function of temperature T recorded at E6: Triangles and squares denote the scattering intensity in a (111) reflection while cycling cD_2 through the liquid-solid transition. Stars and circles illustrate scattering intensity in a (002) reflection.

The growth of the nuclei supposedly follows a Volmer-Weber mode [32] that is the growth of individual initially well-separated embryonic islands. The roughness of the pore walls and the decreasing van der Waals attraction between substrate and nuclei as they grow in size, seem to object other growth modes as layer-by-layer (Frank–van der Merwe) or step-flow [32]. Preferred nucleation sites for the embryonic D_2 islands might be crystallographic low energy facets of pore walls [33,34]. Their influence on textural growth of alcane crystals in pSi has been discussed earlier by Henschel [11].

One should note that Wallacher and Knorr [35] proposed nucleation of crystals in the center of tubular pores in heterogeneous substrates. In their model, a liquid layer between the growing nucleus and substrate was introduced to account for the energetically unfavorable mismatch between the solid and confining host. This approach, however, is not necessarily applicable to the studied system as matching crystallographic structures between substrate (cubic) and condensate (cubic) should strongly favor epitaxial overgrowth of solid D_2 on the pore walls over free nucleation in the pore center.

The reflection widths in Fig. 2 indicate via the Debye-Scherrer equation that only nanometer-sized crystals smaller than 5 nm grow in the confinement. The size of the crystals in radial direction is naturally restricted by the radius of the tubular nanochannels. The size limitations even along the pore axis can be of multiple origin. In accordance with the Volmer-Weber-growth mode, crystalline islands might nucleate with a faster rate than the growth of a single nucleus thus limiting the size of individual crystals. Further, the simultaneous growth of a multitude of D_2 crystals inside pSi is certainly impaired by geometric restrictions due to spatial confinement, the mismatch of lattice constants between Si and D_2 (5% at 1.7 K), pronounced roughness of the crystalline substrate, and random double positioning. As a consequence, defects and strains should develop in the D_2 crystals and reduce also the structural coherence length. The increased lattice constant of cD_2 ($a_c > a_b$) implies directly a strained state of the pore-confined solid. The advent of the rotated domains itself provides additional evidence for strain impaired crystal growth. As fcc crystals grow inside the nanochannels (111) deformation twins form to relieve upcoming strains. Twin and original crystal are related via a rotation of 70.32° as a (111) mirror plane is introduced during the twinning process [36]. Consequently, successive twinning of aligned crystals causes first and second order twin crystals, which are rotated by $\Phi^*_{002} = 70.32°$ and $\Phi^*_{002} = 180° - 2 \times 70.32° = 38.94°$ with respect to the seed crystal. In total there are 12 symmetry equivalent slip systems which can cause these kind of twins in a fcc lattice. Not all are probed for in our scattering geometry but should be employed similarly in the crystals as a resort for strain relief.

A rotated domain with $\Phi^*_{002} = 70.32°$ can also be caused by epitaxy if, for instance, the D_2 crystal grows with a $[\bar{1}\,\bar{1}\,1]$ direction perpendicular to a Si (111) facet. Then the Si substrate and D_2 share a common "mirror" plane and "twinning" occurs directly at the Si-D_2 interface. Double positioning boundaries evolve if such a $[\bar{1}\,\bar{1}\,1]$ nucleus grows adjacent to a [111] nucleus. These unfavorable interfaces, however can be eliminated by introducing a coherent twin boundary parallel to the substrate in one of two nuclei [37].

Growth of D_2 (110) facets on Si (111) facets would cause a rotation of $\Phi^*_{002} = 35.26°$. In the margin of error this value might be considered reasonably close to the experimentally observed one. But molecular distances in the (110) and (111) facets are significantly different and object to such an epitaxial growth scenario. There exists no other combination of two low indexed facets in fcc crystals which are rotated by roughly 39° to explain this rotated domain by simple overgrowth.

Deuterium confined in nanometer-wide Si nanochannels solidifies in a fcc phase and not in the hcp structure known from the bulk system. Heterogeneous liquid phase epitaxy inside the nanochannels guides the nucleation and growth of fcc nanocrystals. Grown crystals exhibit well-defined orientations with respect to the crystalline Si matrix. Billions of them align perfectly with respect to each other. Such systems provide a tempting and unique opportunity to study for instance elementary excitations (phonons, magnons) on nanometer-sized length scales under reduced dimensionality without being impaired by random orientations of the employed nanocrystals. In the near future other condensed gases that form fcc or hcp crystals after solidification will be probed for similar structural characteristics in confinement.

*tommy.hofmann@helmholtz-berlin.de

[1] C. R. Martin, Science **266**, 1961 (1994).
[2] H. Hlaing, X. Lu, T. Hofmann, K. G. Yager, C. T. Black, and B. M. Ocko, ACS Nano **5**, 7532 (2011).
[3] K. Rumpf, P. Granitzer, and H. Krenn, J. Phys. Condens. Matter **20**, 454221 (2008).
[4] P. Granitzer and K. Rumpf, Materials **4**, 908 (2011).
[5] J. E. Allen, K. G. Yager, H. Hlaing, C.-Y. Nam, B. M. Ocko, and C. T. Black, Appl. Phys. Lett. **99**, 163301 (2011).
[6] X. He, F. Gao, G. Tu, D. Hasko, S. Hüttner, U. Steiner, N. C. Greenham, R. H. Friend, and W. T. S. Huck, Nano Lett. **10**, 1302 (2010).
[7] Z. Zheng, K.-H. Yim, M. S. M. Saifullah, M. E. Welland, R. H. Friend, J.-S. Kim, and W. T. S. Huck, Nano Lett. **7**, 987 (2007).
[8] X. She, G. Song, J. Li, P. Han, S. Yang, W. Shulong, and Z. Peng, Polym. J. **38**, 639 (2006).
[9] M. Steinhart, S. Zimmermann, P. Göring, A. K. Schaper, U. Gösele, C. Weder, and J. H. Wendorff, Nano Lett. **5**, 429 (2005).

[10] B. D. Hamilton, J.-M. Ha, M. A. Hillmyer, and M. D. Ward, Acc. Chem. Res. **45**, 414 (2012).
[11] A. Henschel, T. Hofmann, P. Huber, and K. Knorr, Phys. Rev. E **75**, 021607 (2007).
[12] H. R. Glyde, Eur. Phys. J. Special Topics **141**, 75 (2007).
[13] T. X. Nguyen, H. Jobic, and S. K. Bhatia, Phys. Rev. Lett. **105**, 085901 (2010).
[14] P. E. Sokol, R. M. Simeo, C. R. A. Brown, W. G. Stirling, M. A. Adams, S. H. Lee, C. Rutiser, and S. Komarneni, Physica (Amsterdam) **241–243B**, 929 (1998).
[15] E. Kim and M. H. W. Chan, Nature (London) **427**, 225 (2004).
[16] D. Wallacher, M. Rheinstaedter, T. Hansen, and K. Knorr, J. Low Temp. Phys. **138**, 1013 (2005).
[17] M. Schindler, Y. Kondo, and F. Pobell, J. Low Temp. Phys. **110**, 549 (1998).
[18] Y. Wang and P. E. Sokol, J. Low Temp. Phys. **83**, 165 (1991).
[19] Y. J. Glanville, J. V. Pearce, P. E. Sokol, B. Newalker, and S. Komarneni, Chem. Phys. **292**, 289 (2003).
[20] Y. Wang, W. M. Snow, and P. E. Sokol, J. Low Temp. Phys. **101**, 929 (1995).
[21] P. E. Sokol, R. T. Azuah, M. R. Gibbs, and S. M. Bennington, J. Low Temp. Phys. **103**, 23 (1996).
[22] X. G. Zhang, J. Electrochem. Soc. **151**, C69 (2004).
[23] T. Hofmann, D. Wallacher, M. Mayorova, R. Zorn, B. Frick, and P. Huber, J. Chem. Phys. **136**, 124505 (2012).
[24] K. Knorr, P. Huber, and D. Wallacher, Z. Phys. Chem. Materialforsch. **222**, 257 (2008).
[25] W. F. Saam and M. W. Cole, Phys. Rev. B **11**, 1086 (1975).
[26] G. Mason, J. Colloid Interface Sci. **88**, 36 (1982).
[27] A. F. Schuch and R. L. Mills, Phys. Rev. Lett. **16**, 616 (1966).
[28] T. Hofmann, D. Wallacher, P. Huber, and K. Knorr, J. Low Temp. Phys. **140**, 91 (2005).
[29] I. Silvera, Rev. Mod. Phys. **52**, 393 (1980).
[30] K. F. Niebel and J. A. Venables, Proc. R. Soc. A **336**, 365 (1974).
[31] B. Borden and C. Radin, J. Chem. Phys. **75**, 2012 (1981).
[32] M. Herman, W. Richter, and H. Sitter, *Epitaxy* (Springer, Berlin, 2004).
[33] G. Müller, M. Nerding, N. Ott, H. P. Strunk, and R. Brendel, Phys. Status Solidi **197**, 83 (2003).
[34] D. J. Eaglesham, A. E. White, L. C. Feldman, N. Moriya, and D. C. Jacobson, Phys. Rev. Lett. **70**, 1643 (1993).
[35] D. Wallacher and K. Knorr, Phys. Rev. B **63**, 104202 (2001).
[36] R. W. Cahn, Adv. Phys. **3**, 363 (1954).
[37] F. Chien, S. Nutt, J. Carulli, N. Buchan, C. Beetz, and W. Yoo, J. Mater. Res. **9**, 2086 (1994).